Journal of Applied Fluid Mechanics, Vol. 13, No. 1, pp. 335-347, 2020.
Available online at www.jafmonline.net, ISSN 1735-3572, EISSN 1735-3645.
DOI: 10.29252/jafm.13.01.29942

Computational Predictions of Velocity Ratio and Ejection Angle on Purge Flow in a Linear Turbine Cascade with Upstream Disturbance

S. Babu† and S. Anish

Turbomachinery Laboratory, Mechanical Department, National Institute of Technology, Karnataka, 575025, India

†*Corresponding Author Email: sushanlalbabume@gmail.com*

(Received December 21, 2018; accepted May 6, 2019)

ABSTRACT

Secondary air bled from the compressor which bypasses the combustion chamber is used to seal the turbine components from incoming hot gas. Interaction of this secondary air or purge flow with the mainstream can alter the flow characteristics of turbine blade passage. An in depth analysis of secondary loss generation by purge flow in the presence of upstream disturbances has huge relevance. The objective of present study is to understand the aerodynamic and thermal effects caused by the purge coolant flow in the presence of an upstream wake. A linear turbine cascade is selected for the computational study and a stationary cylindrical rod which resembles the trailing edge of nozzle guide vane is kept 20 mm before the leading edge to generate the upstream wake (or disturbance). Purge flow disturbances includes strong formation of Kelvin-Helmholtz vortices at trailing edge and additional roll-up vortices at leading edge. Detailed analysis is carried out by varying the velocity ratios as well as the ejection flow angle. Higher velocity ratio and perpendicular coolant ejection reduces the mainstream axial momentum which enhances the passage cross flow. Even though the mass averaged total pressure loss is linearly dependent on the velocity ratio, a reduction in the ejection angle brings down the loss coefficient at the blade exit. A lower ejection angle will improve the film cooling effectiveness also. The presence of purge flow causes an increase in the overturning and underturning.

Keywords: Secondary vortex; Q Criterion; Film cooling effectiveness; Ejection angle; Exit yaw angle.

NOMENCLATURE

C_{ax}	axial chord length
C_p	normalized static pressure
C_{po}	local total pressure loss coefficient
$\overline{C_{po}}$	pitch averaged total pressure loss coefficient
$\overline{\overline{C_{po}}}$	mass averaged total pressure loss coefficient
CV	counter vortex
H	total span
HPV	hub passage vortex
HPL	pressure side leg of HSV
HSL	suction side leg of HSV
HSV	horse-shoe vortex
LE	Leading edge
m_c	mass flow rate at coolant inlet
m_∞	mass flow rate at mainstream inlet
M	velocity ratio
PS	pressure Side
P_s	static pressuer
P_t	total pressure
$P_{t,c}$	total pressure at coolant inlet
$P_{t,\infty}$	total pressure at mainstream inlet
Re	Reynolds number
SS	Suction Side
T	absolute temperature
T_{aw}	adiabatic wall temperature
T_c	coolant inlet temperature
T_∞	mainstream inlet temperature
TE	trailing edge
U_c	coolant average inlet velocity
U_∞	mainstream average inlet velocity
μ	dynamic viscosity
ρ_c	coolant density
ρ_∞	mainstream air density

η	film cooling effectiveness	α	angle of attack

1. INTRODUCTION

In gas turbines there exists an unavoidable gap between the rotor and stator disk, usually known as seal gap, through which the hot ingress will takes place. To minimize the ingress a sealant flow bled from the compressor is fed through the seal gap which purges and reduces hot ingress and provides endwall cooling. Though it helps in the cooling, the purge flow disturbs the main flow aerodynamics and the flow structure which in turn enhances the secondary flows.

Several experimental and computational studies has been reported focusing on the interaction between purge flow and main annulus flow upstream of the stator and rotor blades.

Blair (1974) attributed the influence of endwall-suction side corner vortex over the strong variations of heat transfer characteristics at blade trailing edge. Also stated that, this corner vortex influence was unaffected by the upstream coolant ejection and endwall boundary layer transition location. Various endwall configurations with upstream slot injection were conducted by Burd and Simon (2000). They stated that traverse pressure gradient leads to the accumulation of coolant at suction-endwall corner for low blowing rates while better coolant coverage was observed for higher blowing rates. McLean *et al.* (2001) explored various modes of coolant injection into mainstream (root, impingement and radial) and found reduction in exit flow angle for root injection and an increase for other two modes.

Numerous studies on the effects of cavity flow over stage efficiency drop were reported in recent years. Reid *et al.* (2006) performed the impact of interaction between cavity flow and tangential velocity component of mainstream flow over passage loss generation at different coolant flow rates. Increased efficiency loss was observed for higher coolant flow rates. Experimental investigation by Jenny *et al.* (2012) on 1.5 stage turbine facility with contoured endwalls reported 1.3% efficiency deficit per percent of injected purge flow and 18% sensitivity reduction towards purge flow with contoured endwall. They observed increase in flow turbulence with increased streamwise vorticity at higher purge flow rate. In another work Jenny *et al.* (2013) studied spanwise shifting of Hub Passage Vortex (HPV) by downstream blade passing effects at different coolant ejection rates. Similar transient analysis over efficiency deficit and HPV spanwise penetration were conducted by Regina *et al.* (2015) on the same turbine facility. They observed an efficiency drop of 0.8% per percent of injected purge flow. Flow field measurement by Schrewe *et al.* (2011), Schrewe *et al.* (2013) exhibits 0.6% efficiency drop for an increase of 1.7% coolant mass flow. They noticed aerodynamic blade loading variations along the spanwise direction and spatial propagation of leading edge (LE) stagnation pressure field in the seal cavity. Marini and Girgis (2007) investigated the cavity flow interaction with freestream flow in a single stage high pressure (HP) turbine and observed 0.07% increase of stage efficiency for raised leading edge endwall profile compared to recessed model.

A few manuscripts related to unsteady analysis on rotating testrigs with purge flow have been published in recent years. Paniagua *et al.* (2004) observed reduction in the exit mach number at first stage stator exit which alters velocity triangle and subsequent rotor relative incidence. The numerical modeling of the testrig revealed the existence of three flow regimes: subsonic, transonic, supersonic (Pau and Paniagua, 2010). Pau *et al.* (2010) analysed the effects of shock structures downstream of stator over disk space static pressure distribution and 50% reduction of pressure fluctuation inside the wheel space were noticed. Ong *et al.* (2012) noticed 5% spanwise periodic variation of secondary flow structures due to unsteady vane-rotor interaction and secondary flow enhancement due to rotor negative incidence in the presence of purge flow. They achieved a reduction in secondary flow penetration and improved stage efficiency for a higher swirl angle for the coolant ejection. Incomplete merging of incoming distorted shock waves with suction side boundary layer and amplification of turbulent kinetic energy in the rotor passage was explained by Pichler *et al.* (2018).

Dahlqvist and Fridh (2018) analyzed the influence of inlet boundary layer thickening on secondary loss generation at engine operated low velocity ratios. Strengthening of secondary flow structures at hub endwall with increased purge flow rates revealed a direct relationship between exit Mach number and purge swirl angle. Schuler *et al.* (2011) noticed boundary layer thickening for different seal geometries and found that compound seal geometry reduced radial penetration of purge flow into mainstream and also restricts hot gas ingress into the wheel space. This hub passage vortex, radial penetration was also observed by Cui and Tucker (2017) and Chen *et al.* (2018) in the presence of purge flow.

Studies on shrouded rotor tip cavity leakage flows were conducted by Pfau *et al.* (2003) and Rosic *et al.* (2008). They stated that various profiled and non-profiles tip cavity geometries with deflectors exhibited flow field improvements and mixing loss reduction. Schlienger *et al.* (2003) explored the effects of purge flow over pressure fluctuations across the leading edge and trailing edge of a shrouded rotor tip with labyrinth seal. They observed breaking of fluid inside the seal exit cavity into low momentum distinct oblique jets which causes additional secondary losses inside the blade passage. Zerobin *et al.* (2018) experimentally studied the

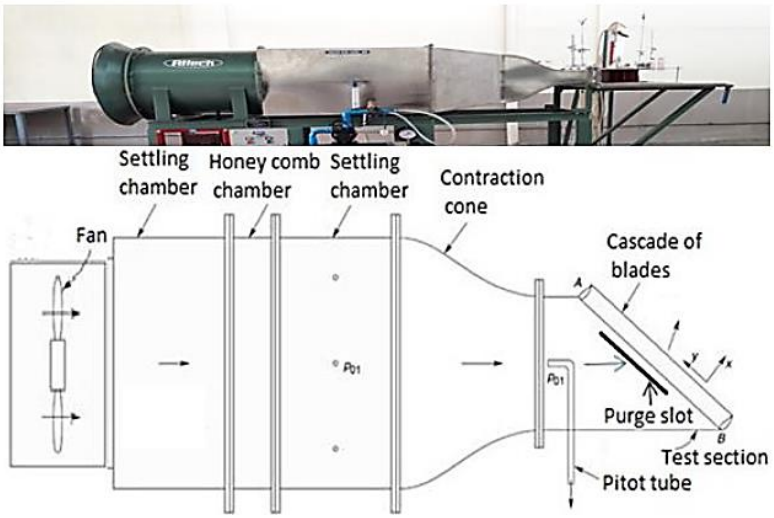

Fig. 1. Experimental test facility.

Turbine Centre Frame (TCF) performance by individually controlling the forward and aft, hub and tip cavity flows and stated that both sealant flow, hub and tip at the High Pressure Turbine (HPT) rotor exit is the major parameter which controls the overall TCF performance. Numerical analysis of the same test facility by Sanz *et al.* (2018) revealed the influence of purge flow over secondary flow loss cores especially tip leakage vortex.

From the literature review it is understood that even though purge flow disturbs the main flow significantly, it is essential for providing the necessary cooling in the disk space. Hence quantifying the extent of loss generation with purge flow is really important, especially in the presence of an upstream disturbance. The objective of the current study is to analyze the influence of the upstream wake combined with purge flow on blade aerodynamics and film cooling effectiveness on the stator passage. Coolant is ejected through a rectangular slot upstream of a linear cascade of high pressure turbine blades at different velocity ratios (M) and ejection angles. Wakes from the preceding blade rows are simulated using stationary cylindrical rod. Secondary flow losses inside the blade passage and exit flow angle deviations are analyzed in detail and comparative study has been made. Practical possibility of passing wakes is outside the scope of this paper and current objective is only to explore the interaction of a standing upstream wake with the purge flow.

2. METHODOLOGY

Experiments are performed in the subsonic wind tunnel (Fig. 1) equipped with linear turbine cascade available at the NITK turbomachinery laboratory. The test section (Fig. 2) is equipped with five turbine blades in a linear configuration mounted between two side walls. A minimum of five blades are used in order to improve the periodicity of the flow. Detailed specifications of the cascade are given in Table 1. Different computational models have been generated and are shown in Fig. 3. In the base case model (Fig. 3(a)) the effect of purge and upstream wake are absent. This model serves as basis for comparison.

Table 1 Turbine blade parameters

Inlet flow angle	52°
Blade exit angle	-66.3°
Total blade turning angle	118.3°
Blade axial chord length	100 mm
Blade pitch	112 mm
Blade span	120 mm
Re	2×10^5
Zweifel loading coefficient	1.18

Most of the literatures are focused on aerothermal-performance variations with purge flow ejecting perpendicular to mainstream flow. A detailed investigation of purge slot ejection angle other than 90° on endwall cooling effectiveness and secondary losses at different velocity ratios are performed in this paper. Apart from normal ejection angle (90^{o}), 45° ejection angle is tested and compared with the base case (Fig. 3 b & c). The purge flow enters into the cascade without any swirl whereas the mainstream flow is entering at an angle of 52° from axial direction. In order to understand the effects of upstream disturbances, simulations are carried out with upstream wake generated by a vertical cylinder kept at 28 mm upstream of blade leading edge (LE). The cylinder is offset 35% pitch from the stagnation line (Fig. 3(d)). The geometrical modeling and meshing of the computational domain is carried out using ICEM-CFD. Flow through a single blade passage is modeled and translational periodic boundary conditions are specified on side walls. The inlet of the fluid domain is kept at 1.5 times the axial chord (C_{ax}) distance upstream of the blade leading edge and the outlet plane is kept at two times the

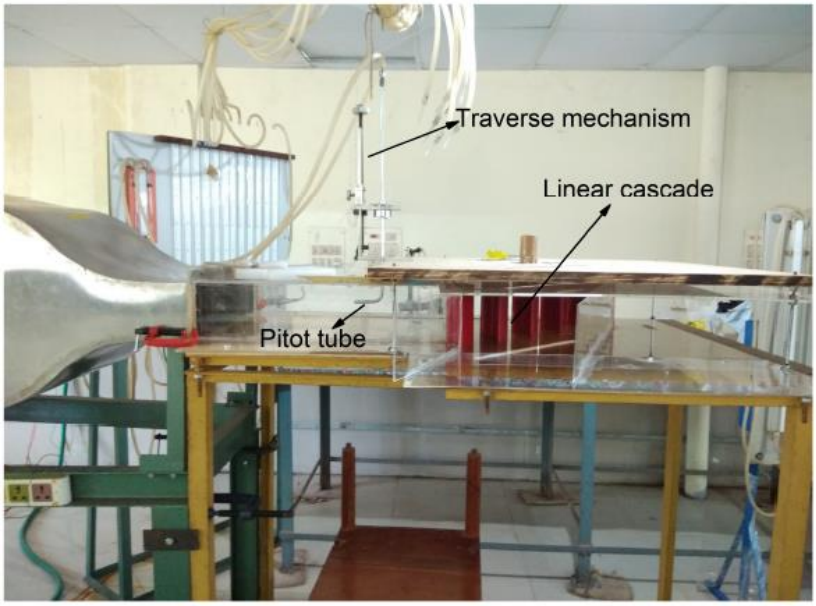

Fig. 2. Test section with linear turbine cascade.

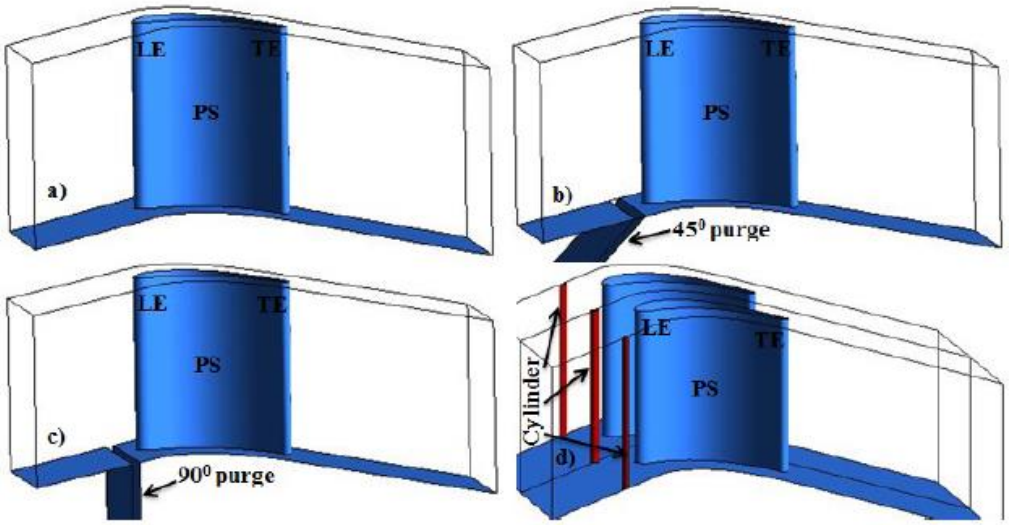

Fig. 3. Computational domains with a) Base case, b) 45° purge, c) 90° purge, d) Base case with upstream cylinders.

axial chord distance downstream of the trailing edge. The grid generation is carried out with fully structured elements and the maximum y+ value is estimated as 2.7 (Fig. 4). The purge slot has a width of 7 mm and is located at 10 mm upstream of the blade leading edge.

Commercial computational fluid dynamics (CFD) solver, ANSYS-CFX is used to solve, the Reynolds Averaged Navier Stokes (RANS) equations. Pressure based solver is used and the turbulence is modeled with SST model. For simulations related to turbine cascade, SST model shows closer match to the experimental data compared to standard k - ε and k - ω models (Jenny *et al.,* 2012; Jenny *et al.,* 2013; Wang *et al.,* 2014; Jia and Liu, 2013). Air as ideal gas is used as the working fluid. Flow variables are solved using high resolution advection scheme. High resolution scheme will attempt to set the order of the scheme as high as possible automatically while keeping the solution bounded everywhere. Boundary layer profile that can provide same boundary layer thickness and momentum thickness as measured in the experiment is provided at the inlet. Table 2. shows the details of inlet boundary layer thickness. 5% turbulence intensity obtained with the help of single sensor hot wire anemometer is specified at the inlet. At the outlet, mass flow rate of 0.28 kg/s is given. At purge flow inlet, velocity inlet boundary condition is given. At one pitch distance translational periodic boundary condition is specified.

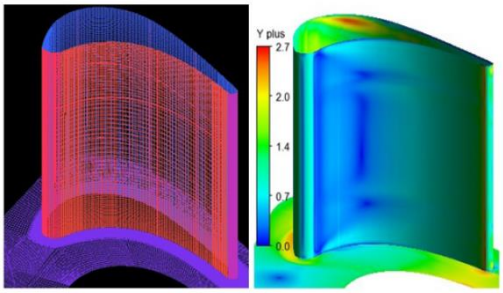

Fig. 4. Structured mesh and Y+ distribution over the blade and hub endwall.

Table 2 Details of boundary layer thickness at the domain inlet

Boundary layer thickness	10 mm
Displacement thickness	1.25 mm
Momentum thickness	1.01 mm

3. GRID INDEPENDENCE STUDY

In order to optimize the number of mesh elements, grid independent study has been carried out at different mesh sizes (2.95 million, 3.16 million, 3.37 million, 3.58 million, 3.79 million and 3.95 million). The number of mesh elements versus mass averaged total pressure loss coefficient at 135% C_{ax} downstream is shown in Fig. 5. At 3.58 million mesh elements, variation in the mass averaged total pressure loss coefficient is 0.36% in comparison with the finest mesh (3.95 million). Hence it has been selected for the base case domain. Similarly optimum mesh size has been identified for other computational models and it is found to be 3.74 million and 4.13 million for purge and purge with cylinder respectively.

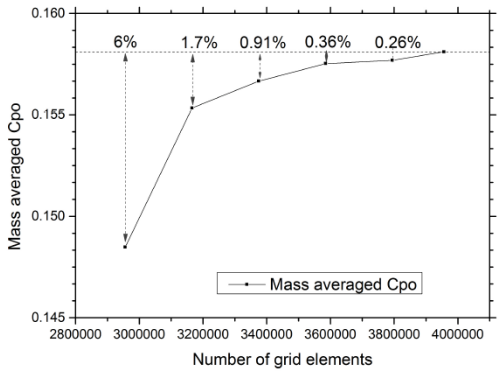

Fig. 5. Grid Independence study for base case. The variation of mass averaged total pressure loss coefficient is shown against various number of grid elements.

4. VALIDATION

The validation of the numerical method is carried out for the base case. Normalized static pressure coefficient (C_p) distribution around the blade surface at three different inlet velocities (14.42 m/s, 19.23 m/s and 24.04 m/s) and local total pressure loss coefficient (C_{po}) distribution at 148% C_{ax} at 29% and 8% span are calculated and compared with the experimental results. Midspan of the blade is equipped with static pressure ports and the C_p obtained from these static ports quantitatively and qualitatively matches with the numerical results (Fig. 6(a)). C_p is calculated by normalizing the static pressure with the inlet dynamic pressure (Eq. (1)). The cascade exit flow field (148% C_{ax}) is traversed with a miniaturized L-shaped five hole probe of head diameter 2 mm having 0.4° accuracy in terms of angles and 0.5% of static and total pressure.

$$C_p = \frac{P_s}{0.5\rho_\infty U_\infty^2} \tag{1}$$

$$C_{po} = \frac{\frac{m_\infty}{m_\infty + m_c}\overline{\overline{P_{t,\infty}}} + \frac{m_c}{m_\infty + m_c}\overline{\overline{P_{t,c}}} - P_t}{0.5\rho_\infty U_\infty^2} \tag{2}$$

The local total pressure loss coefficient (C_{po}) is calculated by Eq. (2), where m_∞ is the mass flow rate at mainstream inlet, m_c is the mass flow rate at coolant inlet, $P_{t,\infty}$ is the total pressure at the mainstream inlet, $P_{t,c}$ is the total pressure at the coolant inlet and Pt is the total pressure at the measuring point. In Fig. 6 b & c , C_{po} distribution is closely matching with the experimental results except at the loss core region. At loss core region, numerical simulations overpredicts the results. This over-prediction is mostly because of the transition nature of endwall boundary layer (Cui and Tucker, 2017). However, a RANS simulation predicts the mean flow behavior with reasonable accuracy (Marini and Girgis, 2007; Aizon *et al.*, 2013; Asghar *et al.*, 2014) and it is very useful in predicting the overall performance analysis of the turbine cascade.

5. RESULTS AND DISCUSSION

5.1 Effect of Purge Flow on Secondary Flow Losses

The simulations have been carried out for different velocity ratios (M=0.2. 0.4, 0.6, 0.8, 1 & 1.2). The velocity ratio (M) is defined as the ratio of coolant inlet average velocity to the mainstream inlet average velocity. The definition of mass averaged and pitch averaged total pressure loss coefficient accounting for the coolant ejection used in this study is given in Eq. (3) and Eq. (4) respectively.

$$\overline{\overline{C_{po}}} = \frac{\frac{m_\infty}{m_\infty + m_c}\overline{\overline{P_{t,\infty}}} + \frac{m_c}{m_\infty + m_c}\overline{\overline{P_{t,c}}} - \overline{\overline{P_t}}}{0.5\rho_\infty U_\infty^2} \tag{3}$$

$$\overline{C_{po}} = \frac{\frac{m_\infty}{m_\infty + m_c}\overline{\overline{P_{t,\infty}}} + \frac{m_c}{m_\infty + m_c}\overline{\overline{P_{t,c}}} - \overline{P_t}}{0.5\rho_\infty U_\infty^2} \tag{4}$$

Figure 7 shows $\overline{\overline{C_{po}}}$ distribution within the blade

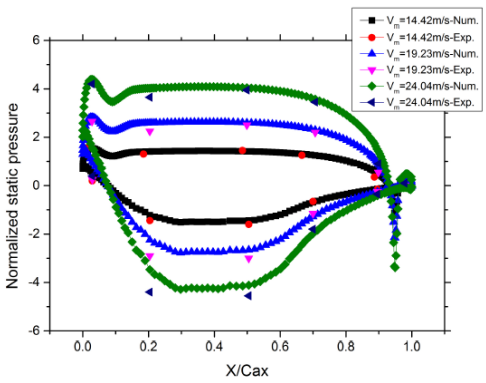

(a) C_p ploted at blade midspan.

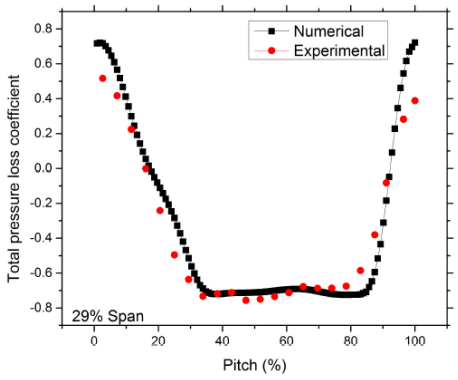

(b) C_{po} ploted at 148% C_{ax} & 29% span.

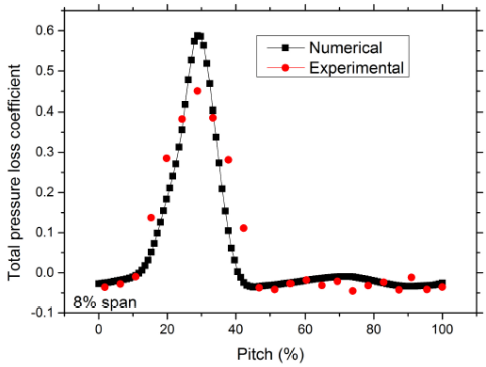

(c) C_{po} ploted at 148% C_{ax} & 8% span.

Fig. 6. Comparison of computational results with the experimental results.

passage along the axial direction for 90° purge.

At each axial location total pressure is mass averaged over the measuring plane and it accounts for all the losses including the mixing effects of purge flow with mainstream flow. With an increase in the value of *M* the rate of increase of loss coefficient also increases. In other words, slope of each curve increases with an increase in *M*. The disturbances created by the purge flow is quite evident from these plots. The dissimilar velocity distribution between mainstream flow and purge flow is the primary cause for the disturbances. Near to the trailing edge (particularly after 90% C_{ax}) the slope of the curve again changes and a rapid increase in the loss coefficient is noted, even with the base case. In an effort to reduce losses, the purge flow angle has been modified to 45°. It was observed that the loss generation has reduced by 5.5% in comparison to the 90° purge angle (Fig. 8) for *M*=0.2. Ejection of coolant at an inclination of 45◦ provide enough acceleration and momentum to the fluid inside the boundary layer for minimizing the cross flow from pressure side to suction side.

The pitch averaged total pressure loss coefficient ($\overline{C_{po}}$) distribution along the span of blade at 135% C_{ax} is calculated and is shown in Fig. 9. The loss coefficients are evaluated from the hub wall to the midspan of blade. Three prominent loss regions are identified and they are endwall loss region, passage vortex (HPV) loss region and counter vortex (CV) loss region. Ligrani *et al.* (2017) identified the passage vortex as pressure side leg of horseshoe vortex (HSV), traversed from pressure to suction side of blade as a result of cross flow. The counter vortex loss core is the suction side leg of HSV dragged into the nearby passage vortex but with opposite sense of rotation. It is observed that the value of loss coefficients rapidly decreases from the endwall up to a span of 4%. The purge flow cases are showing lower losses than base case near the endwall due to the momentum transferred to the boundary layer by the energized coolant ejecting out of purge slot. The losses become significantly higher after a spanwise distance of 15% with the purge flow. Unlike the base case the peak loss coefficient occurs at 25% of span for 45° ejection as well as 90° ejection. These variations suggest that the presence of purge flow has enhanced the passage vortex even though it decreases the losses near the endwall.

Figure 10 shows the surface streamlines superimposed with normalized static pressure contours of endwall for different cases. For the base case stagnation point can be viewed in front of leading edge and separation lines reaches the suction surface at mid of the blade passage. Introduction of

purge flow has completely modified the upstream passage flow field. Difference in the velocity magnitudes between purge and mainstream , pushed the stagnation point towards suction side from leading edge and reattachment point (S1) is pulled upstream by the additional roll-up vortices formed at the leading edge by purge flow. However compared to 90° purge , lower ejection angle, 45° has accelerated the boundary layer fluid shifting the reattachment point more towards the aft part of the blade passage. Additional votrices generated by the purge flow combines with the one generated by cross flow enhances the strength of passage vortex.

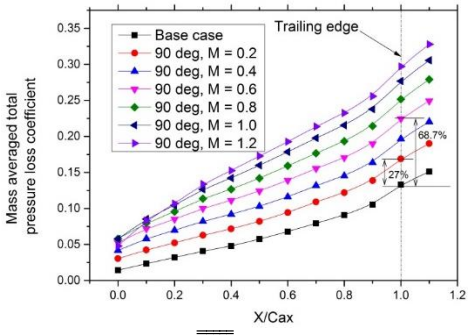

Fig. 7. Variation of $\overline{\overline{C_{po}}}$ distribution along axial direction for 90° purge at different velocity ratios.

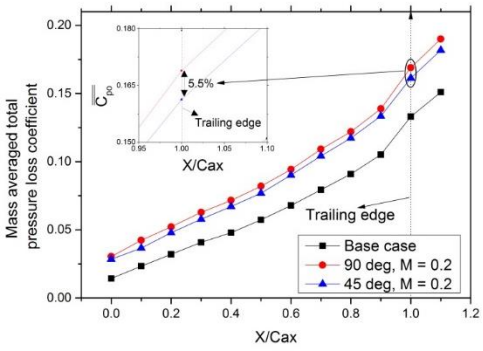

Fig. 8. Variation of $\overline{\overline{C_{po}}}$ distribution along axial direction for 90° and 45° purge at *M*=0.2.

5.2 Effect of Upstream Wakes

The effects of an upstream standing wakes on total pressure loss coefficient and exit yaw angle is presented in this section. The analysis has been carried out for a velocity ratio of *M*=0.2. Mass averaged total pressure loss coefficient at various axial locations is shown in Fig. 11. The addition of an upstream wake causes an increase in the loss by 15% at trailing edge (TE). The interaction of upstream wake with purge flow results in an increase in the loss generation by 21% and 27% for coolant ejection angle of 45° and 90° respectively at the trailing edge. Changing the coolant ejection angle from the normal direction to 45° has resulted in a loss reduction of 6%. The upstream wakes and its interaction with the purge flow enhances mixing losses within the blade passage. Velocity deficit of the mainstream caused by the incoming wakes and secondary flows are the reason for additional loss generation.

The pitch averaged total pressure loss coefficient along the span of blade at 135% C_{ax} is calculated for all the models with upstream standing wake and is shown in Fig. 12. The loss coefficients are evaluated from the hub to the midspan of the blade. The presence of an upstream wake generates additional losses whose effects are visible from 5% span onwards. Slight decrease in the passage vortex losscore is observed around 22% span for both 90° & 45° upstream wake cases. However the total loss coefficient inside the blade passage is increased by the additional vortices. This is explained detail in the following section.

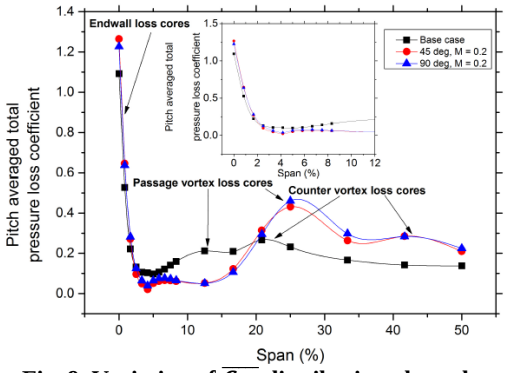

Fig. 9. Variation of $\overline{C_{po}}$ distribution along the span for 90° and 45° purge at 135% C_{ax} for *M*=0.2.

5.3 Vortex Formation at Leading Edge

Figure 13 explains the Q criterion iso surface within the blade passage to visualize the effects of upstream wakes and purge flow for different cases. In general the flow decelerates at the leading edge, due to a radial variation in stagnation pressure. Due to this radial pressure gradient at leading edge, the flow is directed towards the endwall and horse-shoe vortex develops and leads to the formation of hub passage vortex (Fig. 13(a)). Apart from this two additional vortex formations are generated. These are vortex generated by upstream cylinder-AV1 (Fig. 13(b)) and vortex developed at exit of the purge slot-AV2 (Fig. 13(c)) whose strength varies with the purge ejection angle. These additional vortices interact with main flow and results in the strengthening and spanwise shifting of hub passage vortex (Fig. 13(d)).

Figure 14 shows the coherent vortical structure by means of the Q criterion on the suction surface to visualize the effects upstream wakes along with purge flow for different cases. Compared to base case, upstream wakes leads to strong flow separation on the suction surface at midspan near to trailing edge (Fig. 14(b), position 1). Also it increases the size of HPV by 2% at TE and at $0.4 < x/Cax < 0.7$ (Fig. 14(b), position 2). Figure 14 - c & d shows the vortical structure for 90° with and without wake. At Trailing Edge, HPV is covering almost upto 30% of

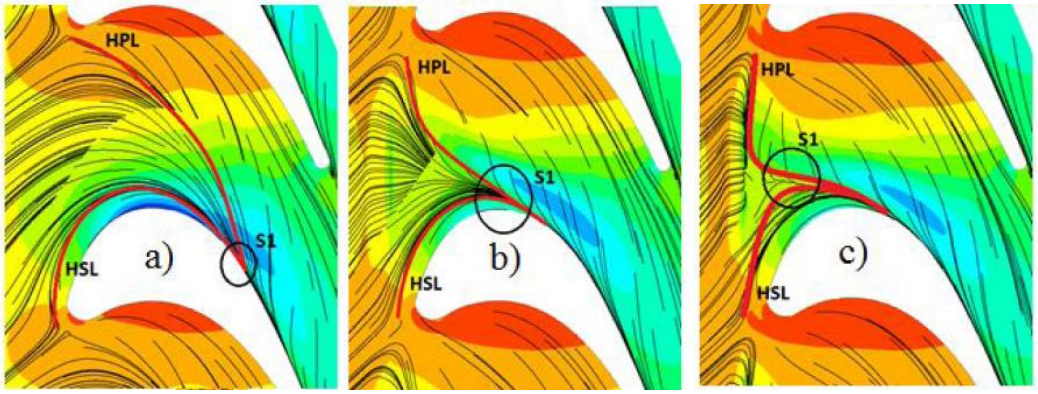

Fig. 10. Endwall surface streamline distribution superimposed with static pressure distribution for a) Base case b) 45° purge & c) 90° purge for *M*=0.2.

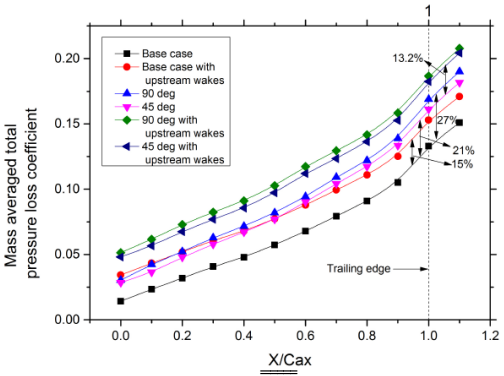

Fig. 11. Comparison of $\overline{\overline{C_{po}}}$ distribution along axial direction for 45° and 90° purge with and without upstream wakes at *M*=0.2.

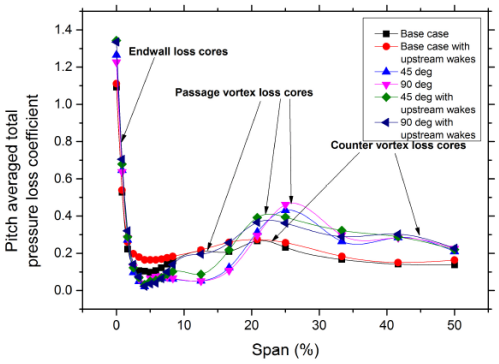

Fig. 12. Variation of $\overline{C_{po}}$ along the span for 45° and 90° purge at 135% C_{ax} with and without upstream wakes at *M*=0.2.

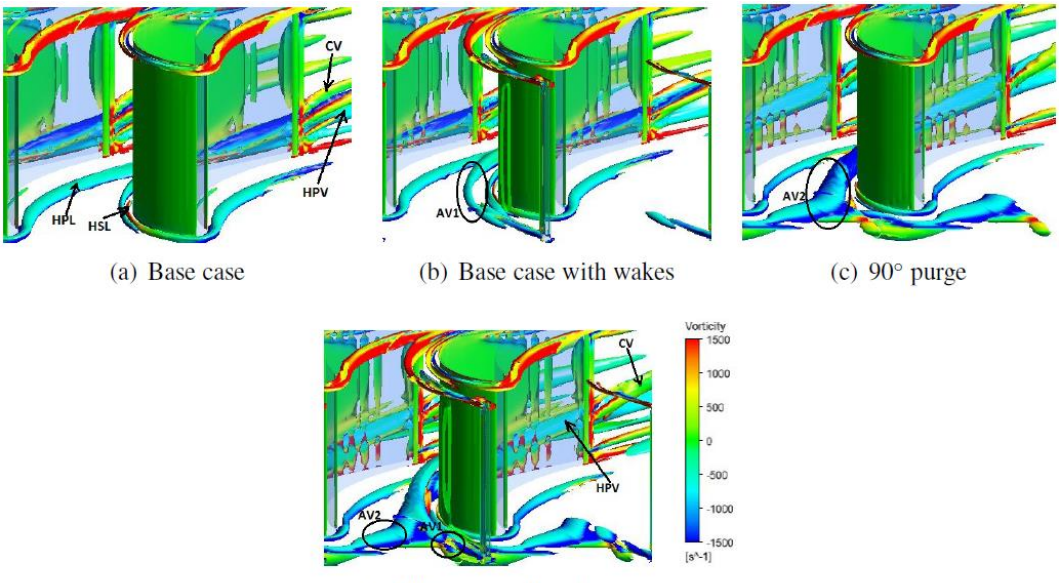

Fig. 13. Vortex formations for different cases.

total span (Fig. 14(c)). Vortex size radially increased 6% between x/Cax, 0.5 and 0.8 (Fig. 14(d), position 3). The normal ejection of coolant (90° purge) to the main stream flow has increased the blockage effect and it enhances the horseshoe vortex formation which in turns leads to high secondary losses. This

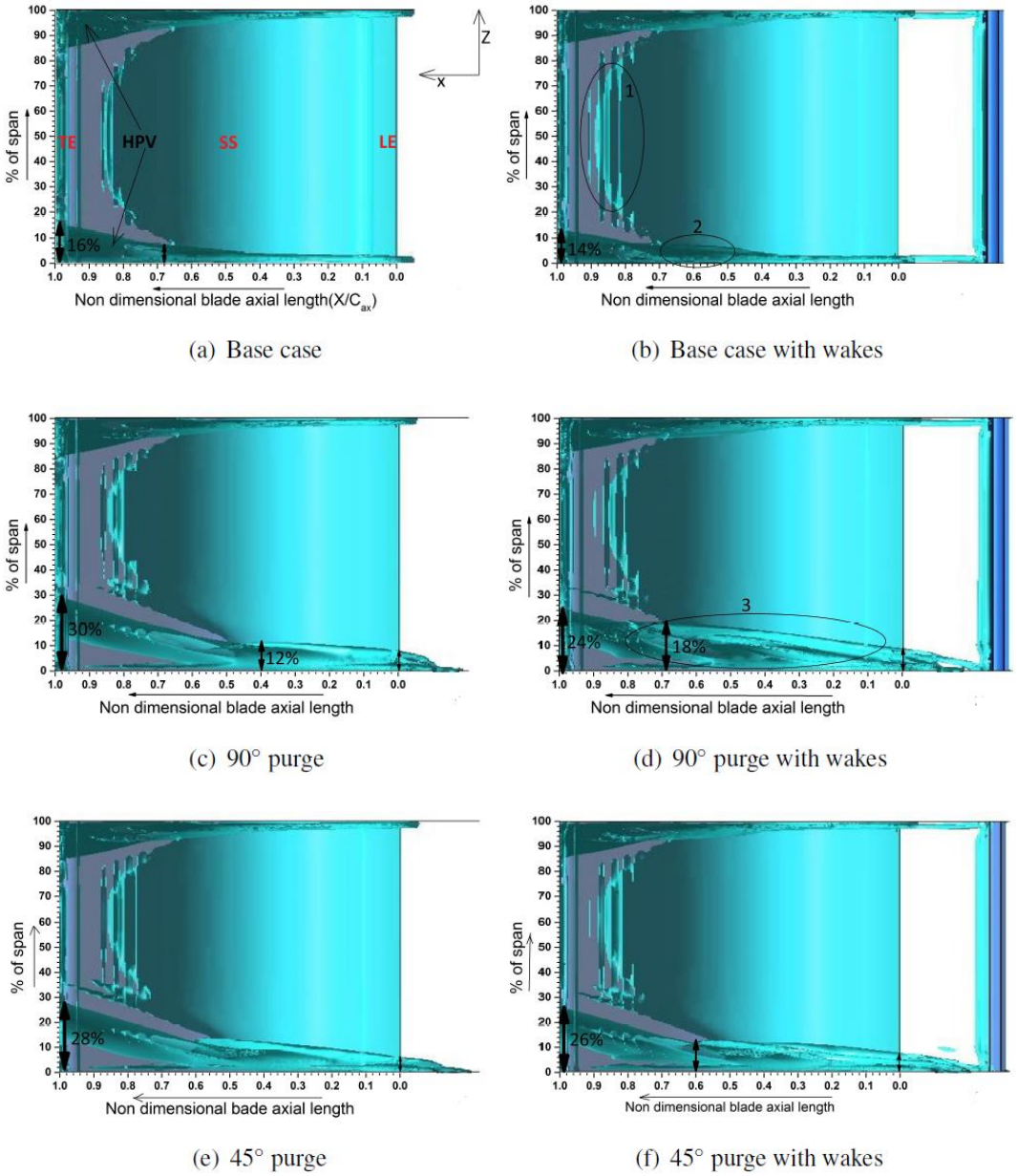

(a) Base case (b) Base case with wakes

(c) 90° purge (d) 90° purge with wakes

(e) 45° purge (f) 45° purge with wakes

Fig. 14. Q criterion iso surfaces for a) Base case, b) Base case with wakes, c) 90˚purge d) 90˚ purge with wakes e) 45˚purge, f) 45˚ purge with wakes.

can be alleviated by making the ejection angle to more horizontal (45˚). The 45˚ purge injection does not disturb the flow significantly and hence it shows 2% reduction in HPV height at trailing edge compared to normal ejection angle (Fig. 14(e)). At leading edge, a radial size reduction for the vortex has been achieved for 45˚ purge compared to 90˚ purge with upstream wakes (Fig. 14(f)). The 45˚ purge flow suppresses the additional losses caused by upstream wakes by adding more momentum to the boundary layer. As a result the flow remains attached to the endwall.

5.4 Effect of Underturning and Overturning

Underturning and overturning has significant effect on the total secondary flow losses. Reduction in both underturning and overturning improves performance of successive blade rows. Figure 15 explains the pitch averaged yaw angle variation for 90˚ purge flow case along the spanwise direction at 135% C_{ax}. The exit yaw angle shows significant variation within the boundary layer and along the span mainly at 20 % and 40% span. The change in yaw angle indicates the variation in the free stream tangential velocity component. At the endwall, the deviation of yaw angle from designed value has reduced significantly for purge cases. However, farther away from the endwall, large variation in yaw angle has been observed. The base case exhibits underturning throughout the span except near the endwall. Whereas the purge flow cases show significant overturning over a span of 15% to 25%, before they enter into underturning.

Figure 16 shows the effects of upstream wakes on exit yaw angle distribution. Close to the endwall all cases exhibit similar trend upto a span of 3 %. However as we move furthers more along the span, purge flow has overturned the mainstream flow beyond the design angle. The differences in the flow deviation caused by 90° and 45° purge cases are almost insignificant, even though 45° purge is showing marginally better results. To understand the effect of upstream wakes and purge flow ejection angle, yaw angle deviation for both 90° and 45° purge cases are compared with base case. Upstream wakes have increased the overturning peak value beyond 70° and reduced the peak underturning to 56°. The disturbances caused by wakes inside the boundary layer has strengthened the cross flow by reducing the free stream momentum. The obvious velocity deficit inside the boundary layer is surpassed by 45° ejection angle. As a result, near the end wall region, 45° purge case with upstream wakes have reduced the exit flow angle around 2° upto the span of 10% and increased the value around 3° upto the span of 33%, when compared to 90° purge case.

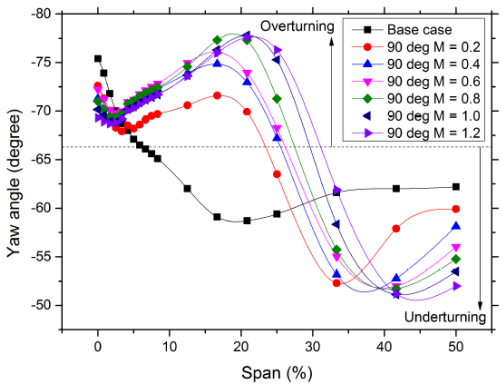

Fig. 15. Pitchwise averaged exit flow angle deviation along the span for 90° purges at *M*=0.2.

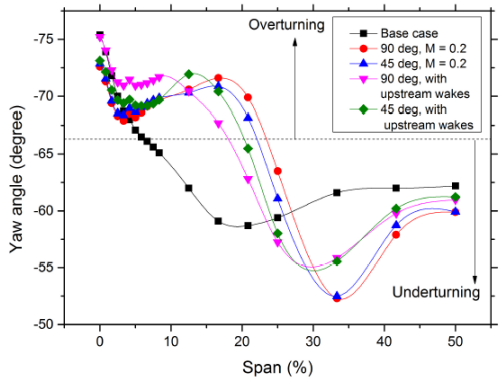

Fig. 16. Effects of upstream wakes on pitch averaged exit flow angle deviation along the span for 45° and 90° purges at 135% C_{ax}.

5.5 Effects on Film Cooling Effectiveness

For the analysis of film cooling effectiveness (FCE), an adiabatic no-slip wall boundary condition is given to the hub endwall. In the present analysis FCE is defined as

$$\eta = \frac{T_\infty - T_{aw}}{T_\infty - T_c} \tag{5}$$

where T_∞, T_{aw} and T_c represents mainstream inlet temperature, adiabatic wall temperature and coolant inlet temperature respectively.

Figure 17 shows the direct comparison of FCE distribution for 90° purge with different velocity ratios. The area covered by coolant over the endwall increases with increase in velocity ratio and with a higher momentum it can surpass the cross flow within the blade passage. For velocity ratio less than 0.4 coolant ejection from the purge slot is not uniform. Particularly for velocity ratio 0.2, coolant ejection does not takes place in front of the stagnation point leaving endwall area around leading edge fully unprotected. At these low velocity ratios, low momentum coolant is pushed back into the purge slot by the mainstream flow because of radial pressure gradient. Downstream of the blade passage, the film cooling effectiveness has decreased after the mid-chord region due to the cross flow. The hub passage vortex has pushed the coolant towards the blade suction side.

Figure 18 reveals that the cooling effectiveness has improved with 45° purge ejection compared to 90°. At the blade leading edge 45° purge ejection has increased the cooling effectiveness by 52.37% compared to 90° purge for *M*=0.4. Also for higher velocity ratios, the highly energized purge flow expanded the area of coolant coverage giving better protection towards the rear part of the blade passage. Effects of upstream wakes on film cooling effectiveness for 90° purge at low velocity ratio (*M*=0.4) is insignificant. on the other hand for 45° ejection, wakes has slightly decreased the film cooling effectiveness and the difference can be observed up to 25% of axial chord. For higher velocity ratio profound effects of wakes are visible for 90° purge case. The upstream wakes have reduced the film cooling effectiveness on an average of 11.34%and 0.05% for both 90° and 45° purge respectively. That means at higher velocity ratio, detrimental effects of wakes are reduced by the high momentum coolant ejecting out of 45° purge slot.

6. CONCLUSIONS

In the present study, both inclination of the purge slot and influence of upstream wakes over blade aerothermal performance were numerically investigated. Numerical results are in good agreement with the experimental data obtained for the base case. Upstream wakes are generated by placing stationary cylindrical rods which resembles the trailing edge of preceding blade rows. The interaction effects of upstream wake with the purge flow has been carried out at different velocity ratios. The blockage effects caused by the normal coolant ejection significantly reduced the mainstream axial momentum. The interaction of upstream wakes and

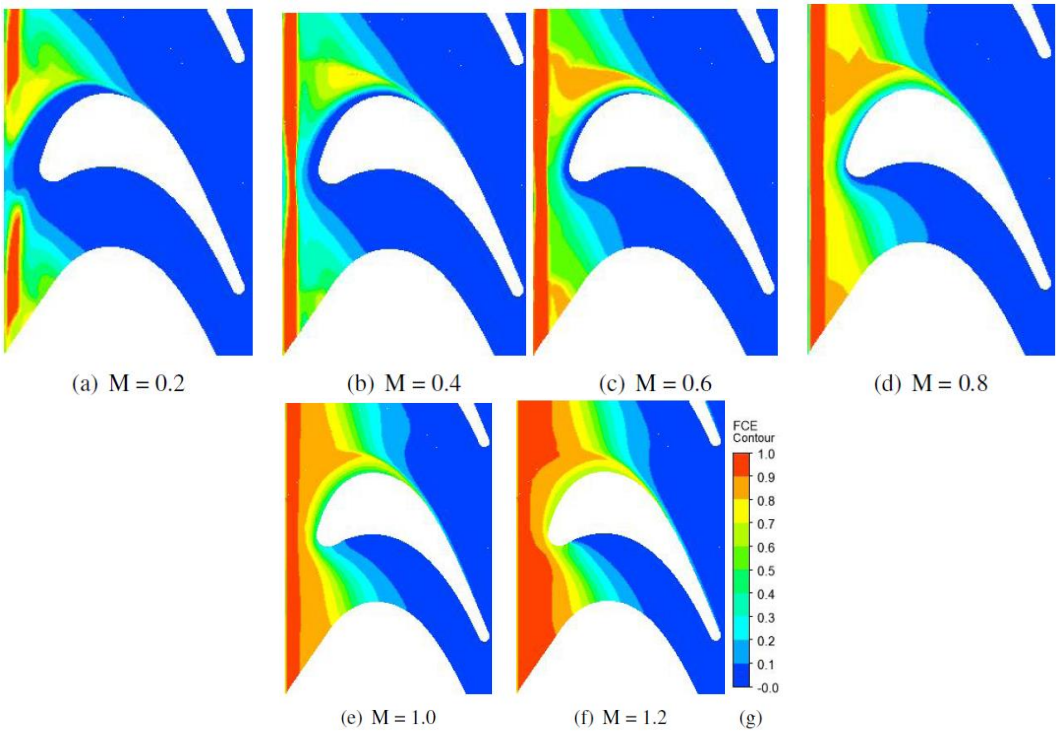

Fig. 17. Local film cooling effectiveness distribution for endwall at 90° purge with different velocity ratios.

purge flow with the low momentum endwall boundary layer has generated additional vortices at the blade leading edge. These additional vortices strengthen the horse shoe vortex and enhances the passage cross flow. In order to reduce the detrimental effects of normal coolant ejection the ejection angle is changed to 45°. Making the ejection angle more horizontal reduces the upstream disturbances compared to a normal ejection. A reduction of 2% in HPV height at trailing edge is achieved for 45° ejection angle. An inclined ejection provides enough acceleration and momentum to the fluid inside the endwall boundary layer to overcome the cross flow from pressure side to suction side resulting a reasonable reduction in the secondary flow losses. Secondary flow restricted most of the coolant ejection to suction side leaving pressure side unprotected. Compared to normal ejection, an inclined ejection of purge flow provides wider coolant coverage and more effectiveness. Reduction of ejection angle to 45° increases the FCE at leading edge by 56.52% for M = 0.6. It is observed that the fore and middle part of blade passages are always protected irrespective of the velocity ratios. However, at low velocity ratio, upstream wakes disturb the film cooling effectiveness for an inclined purge ejection angle. It is also observed that at high velocity ratios cooling effectiveness was not significantly altered by upstream wakes. From the current analysis it is determined that upstream wakes deteriorate the cooling effectiveness at the aft part of the blade endwall. This reveals the obvious need for an additional end wall cooling techniques required for complete protection. The result obtained in this paper depends on specific turbine geometry and care should be taken while generalizing the results.

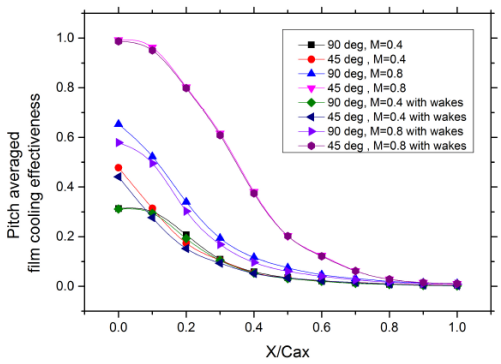

Fig. 18. Effects of wakes on pitch averaged film cooling effectiveness.

ACKNOWLEDGMENTS

The authors gratefully acknowledge the technical support by National Institute of Technology Karnataka (NITK) and financial support by Department of Science and Technology (DST), Ministry of human resource development.

REFERENCES

Aizon, W. G. W., K. I. Funazaki and T. Miura (2013). Purge flow effect on aerodynamics

performance in high-pressure turbine cascade. *Journal of Mechanical Science and Technology* 27(6), 1611–1617.

Asghar, A., W. Allan, M. LaViolette and R. Woodason (2014). Influence of a novel 3d leading edge geometry on the aerodynamic performance of low pressure turbine blade cascade vanes. In *ASME Turbo Expo 2014: Turbine Technical Conference and Exposition*, V02CT38A024 – V02CT38A024. American Society of Mechanical Engineers.

Blair, M. (1974). An experimental study of heat transfer and film cooling on large-scale turbine endwalls. *In ASME 1974 International Gas Turbine Conference and Products Show*, V01AT01A033–V01AT01A033. American Society of Mechanical Engineers.

Burd, S. W. and T. W. Simon (2000). Effects of slot bleed injection over a contoured endwall on nozzle guide vane cooling performance: Part iflow field measurements. In ASME Turbo Expo 2000: Power for Land, Sea, and Air, V003T01A007–V003T01A007. American Society of Mechanical Engineers.

Chen, A. F., C. C. Shiau and J. C. Han (2018). Turbine blade platform film cooling with fan-shaped holes under simulated swirl purge flow and slashface leakage conditions. *Journal of Turbomachinery* 140(1), 011006(1-11).

Cui, J. and P. Tucker (2017). Numerical study of purge and secondary flows in a low-pressure turbine. *Journal of Turbomachinery* 139(2), 021007(1-10).

Dahlqvist, J. and J. Fridh (2018). Experimental investigation of turbine stage flow field and performance at varying cavity purge rates and operating speeds. *Journal of Turbomachinery* 140(3), 031001(1-10).

Jenny, P., R. Abhari, M. Rose, M. Brettschneider and J. Gier (2012). A low pressure turbine with profiled endwalls and purge flow operating with a pressure side bubble. *Journal of Turbomachinery* 134(6), 061038(1-9).

Jenny, P., R. S. Abhari, M. G. Rose, M. Brettschneider, K. Engel and J. Gier (2013). Unsteady rotor hub passage vortex behavior in the presence of purge flow in an axial low pressure turbine. *Journal of Turbomachinery* 135(5), 051022(1-9).

Jia, W. and H. Liu (2013). Numerical investigation of the interaction between upstream cavity purge flow and main flow in low aspect ratio turbine cascade. *Chinese Journal of Aeronautics* 26(1), 85-93.

Ligrani, P., G. Potts and A. Fatemi (2017). Endwall aerodynamic losses from turbine components within gas turbine engines. *Propulsion and Power Research* 6(1), 1-14.

Marini, R. and S. Girgis (2007). The effect of blade leading edge platform shape on upstream disk cavity to mainstream flow interaction of a high-pressure turbine stage. *ASME* Paper No. GT2007-27429.

McLean, C., C. Camci and B. Glezer (2001). Mainstream aerodynamic effects due to wheelspace coolant injection in a high-pressure turbine stage: Part iaerodynamic measurements in the stationary frame. In *ASME Turbo Expo 2001: Power for Land, Sea, and Air*, V003T01A006–V003T01A006. American Society of Mechanical Engineers.

Ong, J., R. J. Miller and S. Uchida (2012). The effect of coolant injection on the endwall flow of a high pressure turbine. *Journal of Turbomachinery* 134(5), 051003(1-8).

Paniagua, G., R. Denos and S. Almeida (2004). Effect of the hub endwall cavity flow on the flow-field of a transonic high-pressure turbine. *Journal of turbomachinery* 126(4), 578-586.

Pau, M. and G. Paniagua (2010). Investigation of the flow field on a transonic turbine nozzle guide vane with rim seal cavity flow ejection. *Journal of Fluids Engineering* 132(11), 111101(1-9).

Pau, M., G. Paniagua, D. Delhaye, A. de La Loma and P. Ginibre (2010). Aerothermal impact of stator-rim purge flow and rotor-platform film cooling on a transonic turbine stage. *Journal of Turbomachinery* 132(2), 021006(1-12).

Pfau, A., J. Schlienger, A. Kalfas and R. Abhari (2003). Unsteady, 3-dimensional flow measurement using a miniature virtual 4 sensor fast response aerodynamic probe (frap). In *ASME Turbo Expo 2003, collocated with the 2003 International Joint Power Generation Conference*, 307–315. American Society of Mechanical Engineers.

Pichler, R., V. Michelassi, R. Sandberg and J. Ong (2018). Highly resolved large eddy simulation study of gap size effect on low-pressure turbine stage. *Journal of Turbomachinery* 140(2), 021003(1-11).

Regina, K., A. Kalfas and R. Abhari (2015). Experimental investigation of purge flow effects on a high pressure turbine stage. *Journal of Turbomachinery* 137(4), 041006(1-8).

Reid, K., J. Denton, G. Pullan, E. Curtis and J. Longley (2006). The effect of stator-rotor hub sealing flow on the mainstream aerodynamics of a turbine. In *ASME turbo expo 2006: power for land, sea, and air*, 789–798. American Society of Mechanical Engineers.

Rosic, B., J. D. Denton and E. M. Curtis (2008). The influence of shroud and cavity geometry on turbine performance: an experimental and computational studypart i: shroud geometry. *Journal of Turbomachinery* 130(4), 041001(1-10).

Sanz, W., S. Zerobin, M. Egger, P. Bader, P.

Pieringer, E. Göttlich and F. Heitmeir (2018). Steady cfd simulation of a high pressure turbine rotor with hub and shroud purge flow. In *ASME Turbo Expo 2018: Turbomachinery Technical Conference and Exposition*, V02BT41A010–V02BT41A010. American Society of Mechanical Engineers.

Schlienger, J., A. Pfau, A. Kalfas and R. Abhari (2003). Effects of labyrinth seal variation on multistage axial turbine flow. In *ASME Turbo Expo 2003, collocated with the 2003 International Joint Power Generation Conference*, 173–185. American Society of Mechanical Engineers.

Schrewe, S., C. Linker, A. Krichbaum and H. Schiffer (2011). Measurements of rim seal mixing processes in an axial two stage turbine. 20th International Symposiumm on Air Breathing Engines (ISABE 2011), Gothenburg, Sweden, Sept, 12–16.

Schrewe, S., H. Werschnik and H. P. Schiffer (2013). Experimental analysis of the interaction between rim seal and main annulus flow in a low pressure two stage axial turbine. *Journal of Turbomachinery* 135(5), 051003(1-9).

Schuler, P., K. Dullenkopf and H. J. Bauer (2011). Investigation of the influence of different rim seal geometries in a low-pressure turbine. In *ASME 2011 Turbo Expo: Turbine Technical Conference and Exposition*, 715–729. American Society of Mechanical Engineers.

Wang, C. Z., S. P. Mathiyalagan, B. V. Johnson, J. A. Glahn and D. F. Cloud (2014). Rim seal ingestion in a turbine stage from 360 degree time-dependent numerical simulations. *Journal of Turbomachinery* 136(3), 031007(1-12).

Zerobin, S., A. Peters, S. Bauinger, A. B. Ramesh, M. Steiner, F. Heitmeir and E. Göttlich (2018). Aerodynamic performance of turbine center frames with purge flowspart i: The influence of turbine purge flow rates. *Journal of Turbomachinery* 140(6), 061009(1-11).